Spin rotation induced by applied pressure in the Cd-doped Ce_2RhIn_8 intermetallic compound

D. S. Christovam,[1] C. Giles,[1] L. Mendonça-Ferreira,[2] J. Leão,[3] W. Ratcliff,[3] J. W. Lynn,[3] S. Ramos,[4] E. N. Hering,[4] H. Hidaka,[5] E. Baggio-Saitovich,[6] Z. Fisk,[7] P. G. Pagliuso,[1] and C. Adriano[1]

[1]*Instituto de Física "Gleb Wataghin," UNICAMP, Campinas-SP, 13083-970, Brazil*

[2]*CCNH, Universidade Federal do ABC (UFABC), Santo André-SP, 09210-580, Brazil*

[3]*NIST Center for Neutron Research, National Institute of Standards and Technology, Gaithersburg, Maryland 20899, USA*

[4]*Departamento de Física, Universidade Federal de Roraima, Boa Vista-RR, 69304-000, Brazil*

[5]*Department of Physics, Hokkaido University, Sapporo, Hokkaido 060-0808, Japan*

[6]*Centro Brasileiro de Pesquisas Físicas, Rua Dr. Xavier Sigaud 150, 22290-180, Rio de Janeiro, RJ, Brazil*

[7]*Department of Physics and Astronomy, University of California, Irvine, California 92697-4574, USA*

(Received 20 July 2019; revised manuscript received 25 September 2019; published 21 October 2019)

The pressure evolution of the magnetic properties of the $Ce_2RhIn_{7.79}Cd_{0.21}$ heavy fermion compound was investigated by single crystal neutron magnetic diffraction and electrical resistivity experiments under applied pressure. From the neutron magnetic diffraction data, up to $P = 0.6$ GPa, we found no changes in the magnetic structure or in the ordering temperature $T_N = 4.8$ K. However, the increase of pressure induces an interesting spin rotation of the ordered antiferromagnetic moment of $Ce_2RhIn_{7.79}Cd_{0.21}$ into the *ab* tetragonal plane. From the electrical resistivity measurements under pressure, we have mapped the evolution of T_N and the maximum of the temperature dependent electrical resistivity (T_{MAX}) as a function of the pressure ($P \lesssim 3.6$ GPa). To gain some insight into the microscopic origin of the observed spin rotation as a function of pressure, we have also analyzed some macroscopic magnetic susceptibility data at ambient pressure for pure and Cd-doped Ce_2RhIn_8 using a mean-field model including tetragonal crystalline electric field (CEF). The analysis indicates that these compounds have a Kramers doublet Γ_7^--type ground state, followed by a Γ_7^+ first excited state at $\Delta_1 \sim 80$ K and a Γ_6 second excited state at $\Delta_2 \sim 270$ K for Ce_2RhIn_8 and $\Delta_2 \sim 250$ K for $Ce_2RhIn_{7.79}Cd_{0.21}$. The evolution of the magnetic properties of Ce_2RhIn_8 as a function of Cd doping and the rotation of the direction of the ordered moment for the $Ce_2RhIn_{7.79}Cd_{0.21}$ compound under pressure suggest important changes of the single ion anisotropy of Ce^{3+} induced by applying pressure and Cd doping in these systems. These changes are reflected in modifications in the CEF scheme that will ultimately affect the actual ground state of these compounds.

DOI: 10.1103/PhysRevB.100.165133

I. INTRODUCTION

The Ce-based heavy fermions materials present unusual and interesting properties arising from the presence of $4f$ electrons and a broad band of conduction electrons. At high temperatures the $4f$ electrons behave as local moments with a Curie-type magnetic susceptibility. As the temperature decreases, these moments start to interact with the conduction electrons to form a fluid of heavy quasiparticles. At low temperature the Ce^{3+} $4f$ electrons experience the effect of competing long-range Ruderman-Kittel-Kasuya-Yosida (RKKY) and short-range Kondo interactions, where both effects are dependent on the coupling constant proportional to the magnetic exchange parameter J_{exch} [1]. Due to this competition the ground state (GS) of the Ce-based compounds can easily be tunable by doping, applied pressure or external magnetic field. This tunability can carry a system from an antiferromagnetic (AFM) state through a quantum phase transition at $T \to 0$ where often unconventional superconductivity appears. In this context it is extremely important to study the effects of doping and applied pressure on the GS of the Ce-based compounds.

The Ce_mMIn_{3m+2} ($M = Co, Rh, Ir$; $m = 1, 2$) series of materials are intensively studied tetragonal variants of the cubic $CeIn_3$ intercalated with m layers of MIn_2 along the c axis [2]. In these structures, the tetragonal crystalline electric field (CEF) splits the Ce^{3+} GS multiplet ($J = 5/2$) into three Kramers doublets (one Γ_6 and two Γ_7s). In fact, the important role of the CEF ground state and/or of scheme of levels for the Ce^{3+} multiplet in affecting the actual GS of these compounds has been heavily explored in the past decades [3–5]. More recently, the GS of the $CeMIn_5$ family ($m = 1$: Ce 115) has been precisely determined by the x-ray absorption (XAS) technique and inelastic neutron scattering (INS) [6,7], where the admixing coefficients of the GS wave function ($|0\rangle = |\Gamma_7^+\rangle = \alpha|\pm 5/2\rangle + \beta\ |\mp 3/2\rangle$) were accurately measured. A pure $|5/2\rangle$ state for Ce^{3+} is a flat orbital in the *ab* plane and it was shown that the $M = Rh$ member has the flatter $4f$ distribution because it presents the larger α value. The authors pointed out the fact that $CeRhIn_5$ is the only member of the 115 family that is not an ambient pressure superconductor. All these studies strongly suggest that the anisotropy of the wave function of the GS may determine the physical properties of the Ce-115 compounds. However, such an analysis has not been done yet in greater detail for the bilayered members of this family.

Apart from the direct determination of the CEF GS wave function and scheme of levels, the determination of the magnetic structure of the HF compounds can also be used to study the symmetry and/or spin anisotropy of the CEF

GS, since the moment's direction can be usually associated with its symmetry properties and magnetic anisotropy. Using magnetic diffraction techniques it is possible to determine the magnetic structure as a function of pressure and doping and extract further information about the evolution of the CEF wave functions of the material. In this work we have performed neutron magnetic diffraction and electrical resistivity measurements under pressure to probe the evolution of the magnetic properties of Ce_2RhIn_8 under the combination of Cd doping and applied pressure effects.

In particular, Cd substitution in the $Ce_mM_nIn_{3m+2n}$ family has previously revealed interesting results for the electronic and magnetic properties of these compounds. For Ce MIn_5 ($m = 1$, $n = 1$) it was found that Cd suppresses the superconductivity for $M =$ Co and Ir while it tends to favor AFM ordering for $M =$ Rh [8,9]. For Ce_2MIn_8 ($m = 2$, $n = 1$: Ce 218) Cd doping increases the T_N for $M =$ Rh and induces a long range magnetically ordered phase for $M =$ Ir [10]. All these previous results suggested that Cd is acting as an electronic tuning agent that induces a decrease of the local density of states at the Ce^{3+} site which tends to reduce the Kondo effect and favor AFM ordering [11,12]. However, previous work on the Ce-218 compounds also exhibited an unexpected increase of the maximum of resistivity measurements (T_{MAX}) when Cd is added to the samples, suggesting a secondary effect of Cd on the system related to changes in the CEF parameters [10].

In this context we also present the temperature evolution of the electrical resistivity measurements on $Ce_2RhIn_{7.79}Cd_{0.21}$ under applied pressure up to 3.6 GPa. With this procedure, we can then try to understand the combined effects of doping and pressure on the microscopic and macroscopic properties of the Ce_2RhIn_8 HF compound.

Finally, to gain further insight into how Cd doping can affect the CEF scheme and GS wave function of the Ce_2RhIn_8 material, we have analyzed previous magnetic susceptibility data [10] from pure and Cd-doped Ce_2RhIn_8 using a mean-field model for a Hamiltonian taking into account the tetragonal CEF and anisotropic interactions between local spins, which act as an effective RKKY interaction [3,13]. From this analysis we were able to extract a plausible trend for the CEF evolution as function of Cd doping for the Ce_2RhIn_8 compound.

II. EXPERIMENTAL DETAILS

Single crystalline samples of $Ce_2RhIn_{7.79}Cd_{0.21}$ were grown by an indium-flux method [14,15]. The tetragonal (P4/mmm) structure and unit cell parameters were determined by x-ray powder diffraction. Electrical resistivity measurements under hydrostatic pressure were carried out in a clamp-type cell using Fluorinert as pressure transmitting medium for $P \lesssim 2.1$ GPa. To $P \sim 3.6$ GPa, the measurements were carried out in a indenter-type cell [16] with Glycerol as trasmitting medium. Pressure was determined by measuring the superconducting critical temperature of a Pb sample. The electrical resistivity was measured using a low-frequency *ac* resistance bridge and four-contact configuration in the temperature range between 0.1 and 300 K. The samples were screened and previously found to be free of surface contamination by residual In flux.

The neutron magnetic diffraction (NMD) experiments were carried out on the BT-9 thermal triple axis neutron spectrometer at the NIST Center for Neutron Research (NCNR). A selected crystal with size of approximately 4 mm × 3 mm × 1 mm was cooled in pumped He with a base temperature of 1.7 K. Neutrons with incident energy $E = 35$ meV were selected using the (002) reflection of a pyrolytic graphite monocromator and filters were used to avoid the higher harmonics. Horizontal collimators of 40-47-40-80 full width at half maximum were employed. The sample was pressurized using a designed aluminium pressure cell with helium gas as the pressure transmitting medium.

III. RESULTS AND DISCUSSIONS

Figure 1 shows the specific heat C_{mag}/T and electric resistivity $\rho(T)$ of the pure and Cd-doped Ce_2RhIn_8 compounds for the crystals used in this work. The results are in good agreement with previous reports [10,17] where it was found that Cd doping shifts the T_N to higher temperatures (see inset).

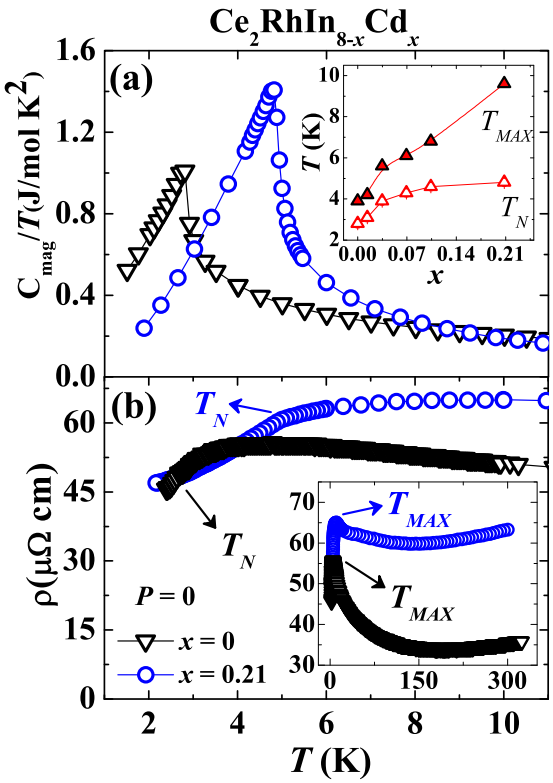

FIG. 1. (a) Magnetic specific-heat data ($C_{mag} = C_T$ - C_{latt}) divided by temperature as a function of temperature for the pure compound (triangles) and doped compound (circles) ($x = 0.21$). The inset presents the evolution of T_N (open triangles) and T_{MAX} (closed triangles) as a function of the Cd concentration, extracted from the temperature dependence of C_{mag} and electrical resistivity $\rho(T)$. (b) Temperature dependence of $\rho(T)$ in the low-T region for the pure (triangles) and doped (circles) ($x = 0.21$) single crystals. The inset in panel (b) shows $\rho(T)$ from 2.0 to about 300 K for both samples. The arrows indicate the temperatures T_N and T_{MAX}, where the electrical resistivity has a maximum.

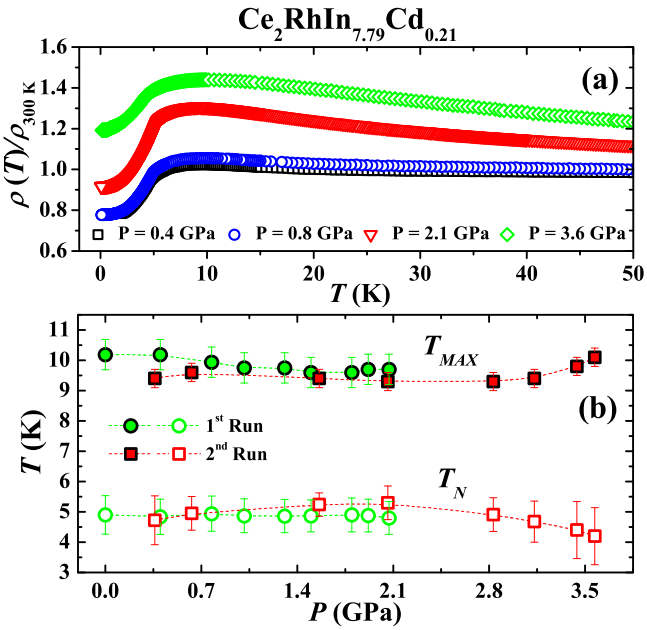

FIG. 2. (a) Temperature dependence of $\rho(T)/\rho_{300K}$ in the low-T region for selected applied pressures. Typical resistivity values for those samples are about 80 $\mu\Omega$ cm. (b) T_N (open symbols) and T_{MAX} (closed symbols) as a function of the applied pressure for $Ce_2RhIn_{7.79}Cd_{0.21}$. Error bars indicated one standard deviation. The first run (circles) was performed in the clamp-type cell, and the second run (squares) was performed in the indenter-type cell. Each run was performed with different single crystals. T_{MAX} was determined from the peaks in the derivative of $\rho(T)$. The dotted lines are a guide to the eyes.

Figure 2 shows the evolution of T_N and T_{MAX} as a function of the applied pressure for $Ce_2RhIn_{7.79}Cd_{0.21}$. From these data one can observe how the properties of the Ce_2RhIn_8 compound changes as a function of the applied pressure. For $P = 0$, a small amount of Cd in the system produces an increase of T_N, which is associated with an electronic tuning [10,18]. However, considering the two pressure runs in Fig. 2, one can say that T_N remains nearly constant as a function of pressure, whereas T_{MAX} slightly decreases for low pressures until it reaches a minimum value $T_{MAX} \sim 9.5$ K at $P \sim 1.4$ GPa. Then it remains nearly constant up to $P \sim 3.0$ GPa and starts to slightly increase up to $P \sim 3.5$ GPa. These unusual behaviors of the T_N and T_{MAX} were also observed for pure $CeRhIn_5$ [19] and Ce_2RhIn_8 [20]. For both materials a minimum in the pressure dependence of T_{MAX} occurred at about 1.5 GPa. For higher pressures T_{MAX} starts to increase as well as a low temperature kink that evolves into a SC transition in both cases. However, in the case of the Cd sample, we have found no evidence for the emergence of a superconducting state in the studied pressure range.

Now we turn to the evolution of the low-T magnetic structure induced by Cd and applied pressure in the AFM state of Ce_2MIn_8 determined by NMD experiments in $Ce_2RhIn_{7.79}Cd_{0.21}$. For these experiments we have selected the samples with the higher T_N of 4.8 K for $x = 0.21$, based on our previous studies [10].

The experiments were performed with an incident energy of 35 meV with no absorption corrections based on the fact

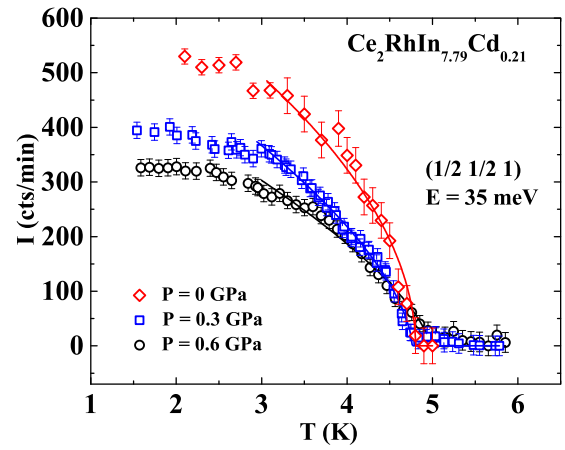

FIG. 3. Temperature dependence of the neutron integrated intensity of the $(\frac{1}{2}, \frac{1}{2}, 1)$ magnetic reflection measured under 0.3 GPa (open squares) and 0.6 GPa (open circles) during heating the sample in the temperature range between $T = 2.0$ K and $T = 6.0$ K for $Ce_2RhIn_{7.79}Cd_{0.21}$. Error bars indicated one standard deviation. The ambient pressure measurement (open diamonds) was adapted from Ref. [10]. The solid curves are a fit to the data using the expression $I/I_0 = (1 - T/T_N)^\beta$, which yields $I_0 = 820(50)$ cts/min, $\beta = 0.5(4)$, $T_N = 4.8(1)$ K for $P = 0$; $I_0 = 680(30)$ cts/min, $\beta = 0.6(3)$, $T_N = 4.8(2)$ K for $P = 0.3$ GPa; and $I_0 = 570(40)$ cts/min, $\beta = 0.7(6)$, $T_N = 5.0(4)$ K, for $P = 0.6$ GPa. These values of T_N are in agreement with resistivity and specific heat measurements.

that at this energy the neutron penetration length is about 2.0 mm, which is longer than the thickness of the sample. Indeed, we have measured Rocking curves for different domains and no significant changes on the intensities were noticed. In a previous work, we determined the magnetic structure of the $Ce_2(Rh, Ir)In_{7.79}Cd_{0.21}$ compounds using x-ray and neutron magnetic diffraction, where we found the propagation vector $(\frac{1}{2}, \frac{1}{2}, 0)$ for both samples and a staggered moment of 0.9(2) μ_B per Ce at 2.0 K, tilted 47(5)° from the *ab* plane, for M = Rh, and a staggered moment of 0.4(5) μ_B per Ce at 2.0 K tilted 21(5)° from the *ab* plane for M = Ir [10].

Here we extended the NMD studies for the $Ce_2RhIn_{7.79}Cd_{0.21}$ to follow its magnetic structure evolution under applied pressure for ambient pressure, $P = 0.3$ and 0.6 GPa. Magnetic peaks were found in the AFM phase at reciprocal lattice points consistent with the $(\frac{1}{2}, \frac{1}{2}, 0)$ propagation vector showing that the pressure is not affecting the relative magnetic interactions between the Ce^{3+} ions.

Figure 3 displays the temperature dependence of the integrated intensity of the $(\frac{1}{2}, \frac{1}{2}, 1)$ magnetic reflection measured between 2.0 and 5.0 K while warming the sample for $Ce_2RhIn_{7.79}Cd_{0.21}$ under applied pressure of $P = 0.3$ GPa (open circles) and $P = 0.6$ GPa (open squares). It is interesting to note that the applied hydrostatic pressures used in the experiment do not significantly change the T_N, in agreement with what was found in the electrical resistivity measurements under pressures for the same sample (Fig. 2).

To completely solve the magnetic structure of the studied samples, the magnetic moment orientation of the Ce^{3+} ion in relation to the crystallographic axis needs to be determined. As such, the integrated intensities of the $(\frac{1}{2}, \frac{1}{2}, l)$ magnetic Bragg peaks were obtained using a Voigt fit in the θ scans.

These magnetic peaks were first normalized using the nuclear Bragg peaks $(00l)$ for $l = 1, 2, 3, 4$, and 7; $(11l)$ for $l = 1, 2, 3, 4, 5$, and 6; and $(22l)$ for $l = 0, 1, 2, 3$, and 6. In barn units the magnetic cross section for a collinear magnetic structure using unpolarized neutrons is given by [21–23]:

$$\sigma(Q) = \left(\frac{\gamma r_0}{2}\right)^2 |S|^2 |f(Q)|^2 \sum_{\mu,\nu} (\delta_{\mu,\nu} - \hat{Q}_\mu \hat{Q}_\nu) \times F^*_\mu(Q) F_\nu(Q), \quad (1)$$

where $(\gamma r_0/2)^2 = 0.07265$ b/μ_B^2, S is the effective magnetic moment of the Ce^{3+} ion, $f(Q)$ is the Ce^{3+} magnetic form factor [24], and $F_\mu(Q)$ is the μ^{th} cartesian component of magnetic structure factor per Ce 218. The calculations were made considering the average of the possible domains and the result is given by [21]

$$\sigma(Q) = \left(\frac{\gamma r_0}{2}\right)^2 |S|^2 |f(Q)|^2 \langle 1 - (\hat{Q} \cdot \hat{z}_n)^2 \rangle |F_M(Q)|^2, \quad (2)$$

where F_M(Q) is the magnetic form factor calculated for the two Ce^{3+} ions of the unit cell along the c axis, $\hat{z}_n$ is the unit vector of the magnetic moment, and the average, $\langle 1 - (\hat{Q} \cdot \hat{z}_n)^2 \rangle$, is over the magnetic domains [21].

As the NMD technique does not allow the moment direction determination in the ab plane due to the square symmetry [22,23], one can only determine the moment direction relative to the c axis. In this case, considering the magnetic moment with an arbitrary orientation in relation to the c axis, there are 16 magnetic domains with tetragonal symmetry and for an equal population of domains, the average term of the Eq. (2) can be written as [21]

$$\langle 1 - (\hat{Q} \cdot \hat{z}_n)^2 \rangle = 1 - \frac{\cos^2\alpha \cos^2\eta + 2 \sin^2\alpha \sin^2\eta}{2}. \quad (3)$$

Here α is the angle of $\vec{Q}$ in relation to the basal plane and η is the angle between the moment direction and the basal plane.

Figure 4 shows the l dependence of the experimental $(\frac{1}{2}, \frac{1}{2}, l)$ magnetic intensities compared with the magnetic cross section $\sigma(Q)$ in mbarn units calculated using the model discussed in Eqs. (1)–(3) for the $Ce_2RhIn_{7.79}Cd_{0.21}$ sample with no applied pressure in Fig. 4(a) and with $P = 0.3$ and 0.6 GPa, respectively, in Figs. 4(b) and 4(c). The solid line in each panel displays the best fit obtained for the magnetic moment direction using the model discussed above for each pressure.

The magnetic structure of $Ce_2RhIn_{7.79}Cd_{0.21}$ was then explored at hydrostatic pressures of 0.3 and 0.6 GPa. The magnetic moment direction determined for this compound with no applied pressure found $\eta = 45(3)^\circ$ and a staggered moment of $S = 0.90(5)\mu_B$, in accordance with previous measurements [10]. The present study under pressure revealed $\eta = 21(3)^\circ$ and $S = 0.85(5)\mu_B$ for $P = 0.3$ GPa and $\eta = 0(3)^\circ$ and $S = 0.80(5)\mu_B$ for $P = 0.6$ GPa. As such, these results shows an evolution of the moment direction toward the ab plane as a function of applied pressure. Also one can see the effective magnetic moment of the ordered phase tends to decrease as a function of the pressure, in accordance with the small variation of T_N in the studied pressure range, which may be associated to the expected enhancement of the Kondo effect as a function of increasing pressure.

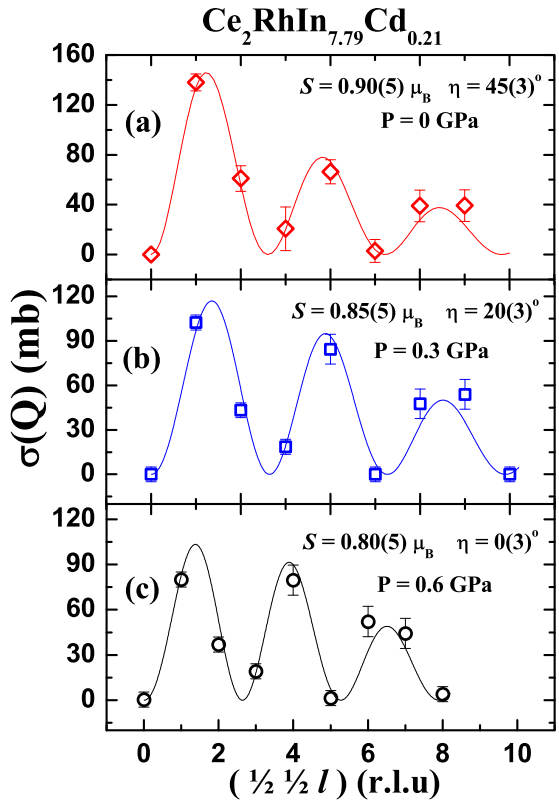

FIG. 4. l dependence (in reciprocal lattice units) of $\sigma(Q)$ for the magnetic peaks $(\frac{1}{2}, \frac{1}{2}, l)$ measured with the neutron energy of 35 meV at $T = 2.0$ K for (a) ambient pressure $Ce_2RhIn_{7.79}Cd_{0.21}$ (open diamonds) and with applied pressures of (b) 0.3 GPa (open squares) and (c) 0.6 GPa (open circles). The solid lines in each panel represent the best fit using the model discussed in Eqs. (1)–(3).

Comparing the evolution of the magnetic structure found by NMD with the electrical resistivity measured under hydrostatic pressure (Fig. 2) one can see that the initial decrease of T_{MAX} roughly coincides with the pressure range for which the magnetic moments are rotating from 45° to the ab plane.

Based on the NMD results one can conclude that the applied pressure has a clear effect on the magnetic structure of the $Ce_2RhIn_{7.79}Cd_{0.21}$ compound, rotating the ordered moment direction toward to the ab plane, which should be associated with changes of the single ion anisotropy and CEF effects.

Determination of the magnetic structure involving the direction of the ordered moments gives an important experimental constraint that can be used to investigate the CEF levels of this compound, along with the anisotropy of the magnetic susceptibility [10]. Therefore, we have tried to gain some insights about the CEF effects in our Cd-doped samples using a theoretical model that has been used in other Ce-based HF [25–27] and 115 compounds [13,28]. This model is based on the Hamiltonian:

$$\mathcal{H} = K_{\text{AFM}} \sum_{i,j} J_i \cdot J_j + B_2^0 O_2^0 + B_4^0 O_4^0 + B_4^4 O_4^4, \quad (4)$$

where $K_{\text{AFM}} > 0$ represents the interaction between nearest neighbor local spins $J_{i,j}$, and the latter terms are the CEF parameters and Stevens equivalent operators (related to the

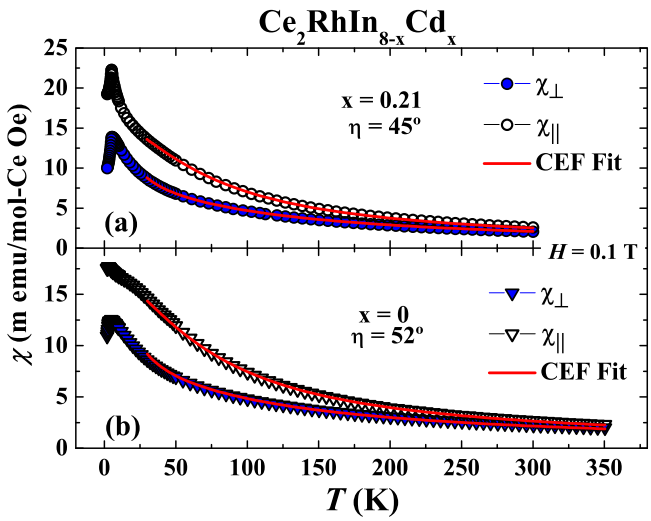

FIG. 5. Magnetic suceptibility data obtained at ambient pressure in an applied field of 0.1 T parallel to the c axis (open symbols) and to the ab plane (closed symbols). The solid lines are the corresponding fits to the CEF model discussed in the text for (a) Cd-doped $Ce_2RhIn_{7.79}Cd_{0.21}$ (circles) and (b) pure Ce_2RhIn_8 (squares). The η angles in the figures were used as a constraint in the CEF fit. Note: 1 emu/(mol Oe) $= 4\pi \times 10^{-6}$ m^3/mol.

angular momentum operators) which are responsible for CEF effects. The operator $O_2^0 = 3\hat{J}_{z,i}^2 - J(J+1)$, for example, favors in-plane alignment for positive B_2^0 or along the c axis for negative B_2^0. With a standard mean-field approximation ($J_iJ_j \sim zJ\langle J\rangle$), where z is the number of nearest neighbors, it is possible to simplify the interaction term of the Hamiltonian to $zK_{\rm AFM}J\langle J\rangle$. We took into account two interactions between nearest and next-nearest neighbors to solve $\mathcal{H}$.

This model was used to fit the paramagnetic susceptibility $\chi(T)$ data for both Ce_2RhIn_8 and $Ce_2RhIn_{7.79}Cd_{0.21}$. The best fit can be seen in Fig. 5, which provides the parameters listed in Table I.

The crystal field parameters in Table 1 were obtained using the rotation of the angle η toward the ab plane as a constraint [10,21]. They provide a good agreement with the characterized magnetic structure and the anisotropy of magnetic susceptibility for both samples. The fit also indicates that the compounds' CEF GS is a $|\Gamma_7^-\rangle = \beta|\pm 5/2\rangle - \alpha\,|\mp 3/2\rangle$ with $\alpha \approx 0.64$, followed by the first excited doublet $|\Gamma_7^+\rangle = \alpha|\pm 5/2\rangle + \beta\,|\mp 3/2\rangle$ at approximately 80 K for both samples and a pure $|\Gamma_6\rangle = |\pm 1/2\rangle$ lying 270 K above the GS for Ce_2RhIn_8 and 250 K above for $Ce_2RhIn_{7.79}Cd_{0.21}$. The CEF splittings for the pure compound are also in good agreement with previous data obtained from thermal expansion experiments [29].

TABLE I. Extracted CEF parameters and exchange interactions between nearest ($K_{\rm Nearest}$) and next-nearest neighbors ($K_{\rm NNN}$) (in kelvin) for Ce_2RhIn_8 and $Ce_2RhIn_{7.79}Cd_{0.21}$. Here the interaction terms are already accounting for the number of neighbors z as in $zK_{\rm AFM}$, and it was suppressed just for the sake of notation simplicity.

CEF parameters for $Ce_2RhIn_{8-x}Cd_x$						
x	T_N	B_2^0	B_4^0	B_4^4	$K_{\rm Nearest}$	$K_{\rm NNN}$
0	2.8	−7.4	0.31	1.5	6.7	0.29
0.21	4.8	−6.9	0.29	1.4	6.9	0.35

Based on these results we can suggest a trend regarding the effect of Cd doping on the CEF scheme of the pure compound. The dopant appears to be decreasing the CEF splittings leading to the variation of the occupation of excited levels, possibly increasing the XY anisotropy of low-lying CEF wave functions for the Cd-doped compound. Since Cd tends to favor a magnetic state as can be seen in Fig. 1(a), one could naively extrapolate the Ce-115 trend in which a flatter orbital distribution (and an AFM ordering in the plane) in the GS would make Cd-doped Ce_2RhIn_8 unlikely to become superconducting even at higher pressure, in agreement with the data of Fig. 2 in the studied pressure range.

It is worth noting that our model is a simple approximation which does not take into account the Kondo interactions which are known to play a role at at low temperature for these materials. Nevertheless, the fits may provide some valuable information about the CEF scheme for the studied compounds, especially with the constraint of the known direction of the ordered moment determined by NMD. Nonetheless, additional experiments such as inelastic neutron scattering, which would be very challenging given the large absorption cross sections, and x-ray inelastic techniques like resonant and non-resonant scattering as well as absorption spectroscopy, particularly in the Cd-doped samples, would be helpful in gathering information about the CEF parameters, and understanding the interesting trends suggested in this work.

IV. CONCLUSIONS

We report the pressure dependence of the low temperature physical properties of a Cd-doped Ce_2RhIn_8 single crystalline sample. The results of heat capacity and electrical resistivity as a function of temperature revealed an enhancement of the T_N from 2.8 K for the pure compound to 4.8 K for $x = 0.21$ of Cd.

We have investigated the effect of applied pressure on the Cd-doped Ce_2RhIn_8 compounds where we have found no changes in the T_N or propagation vector but have revealed a rotation of the ordered moment from 45(3)° (for $P = 0$ GPa) to the ab plane with $P = 0.6$ GPa in $Ce_2RhIn_{7.79}Cd_{0.21}$.

From the analysis of magnetic susceptibility data using the determined direction of the ordered moment as a constraint for pure Ce_2RhIn_8 and $Ce_2RhIn_{7.79}Cd_{0.21}$, we were able fit the data and extract the CEF scheme for both pure and Cd-doped Ce_2RhIn_8. Our results indicate that Cd doping tends to lower the energy of excited states and consequently flatten the orbital distribution of the underlying GS, favoring AFM ordering in these series. These results help to elucidate the trends previously observed for the Ce-115 and Ce-218 compounds where Cd doping acts mainly as an electronic tuning agent changing the local density of states near the Ce^{3+} sites. Although this is certainly the case, this work also shows that both Cd doping and pressure change the CEF scheme. In particular, for $Ce_2RhIn_{7.79}Cd_{0.21}$, these combined effects lead to a more robust AFM state with an ordered moment in the

ab plane, which makes this compound less favorable to host superconductivity under applied pressure.

ACKNOWLEDGMENTS

This work was supported by FAPESP (Grants No. 2006/60440-0, No. 2009/09247-3, No. 2017/10581-1, and No. 2019/04196-3) (SP-Brazil), CNPq (Brazil), and CAPES (Brazil). The staff at the BT-9 instrument are gratefully acknowledged for providing an outstanding scientific environment during these experiments. The identification of any commercial product or trade name does not imply endorsement or recommendation by the National Institute of Standards and Technology.

[1] A. C. Hewson, *The Kondo Problem to Heavy Fermions* (Cambridge University Press, Cambrige, 1993).
[2] J. D. Thompson and Z. Fisk, J. Phys. Soc. Jpn. **81**, 011002 (2012).
[3] A. D. Christianson, E. D. Bauer, J. M. Lawrence, P. S. Riseborough, N. O. Moreno, P. G. Pagliuso, J. L. Sarrao, J. D. Thompson, E. A. Goremychkin, F. R. Trouw, M. P. Hehlen, and R. J. McQueeney, Phys. Rev. B **70**, 134505 (2004).
[4] T. Takimoto, T. Hotta, T. Maehira, and K. Ueda, J. Phys.: Condens. Matter **14**, L369 (2002).
[5] P. G. Pagliuso, N. J. Curro, N. O. Moreno, M. F. Hundley, J. D. Thompson, J. L. Sarrao, and Z. Fisk, Physica B **320**, 370 (2002).
[6] T. Willers, Z. Hu, N. Hollmann, P. O. Korner, J. Gegner, T. Burnus, H. Fujiwara, A. Tanaka, D. Schmitz, H. H. Hsieh, H.-J. Lin, C. T. Chen, E. D. Bauer, J. L. Sarrao, E. Goremychkin, M. Koza, L. H. Tjeng, and A. Severing, Phys. Rev. B **81**, 195114 (2010).
[7] T. Willers, F. Strigari, Z. Hu, V. Sessi, N. B. Brookes, E. D. Bauer, J. L. Sarrao, J. D. Thompson, A. Tanaka, S. Steffen, L. H. Tjeng, A. Severing, Proc. Natl. Acad. Sci. USA **112**, 2384 (2015).
[8] L. D. Pham, T. Park, S. Maquilon, J. D. Thompson, and Z. Fisk, Phys. Rev. Lett. **97**, 056404 (2006).
[9] M. Nicklas, O. Stockert, T. Park, K. Habicht, K. Kiefer, L. D. Pham, J. D. Thompson, Z. Fisk, and F. Steglich, Phys. Rev. B **76**, 052401 (2007).
[10] C. Adriano, C. Giles, E. M. Bittar, L. N. Coelho, F. de Bergevin, C. Mazzoli, L. Paolasini, W. Ratcliff, R. Bindel, J. W. Lynn, Z. Fisk, and P. G. Pagliuso, Phys. Rev. B **81**, 245115 (2010).
[11] R. R. Urbano, B.-L. Young, N. J. Curro, J. D. Thompson, L. D. Pham, and Z. Fisk, Phys. Rev. Lett. **99**, 146402 (2007).
[12] K. Chen, F. Strigari, M. Sundermann, Z. Hu, Z. Fisk, E. D. Bauer, P. F. S. Rosa, J. L. Sarrao, J. D. Thompson, J. Herrero-Martin, E. Pellegrin, D. Betto, K. Kummer, A. Tanaka, S. Wirth, and A. Severing, Phys. Rev. B **97**, 045134 (2018).
[13] P. G. Pagliuso, D. J. Garcia, E. Miranda, E. Granado, R. Lora Serrano, C. Giles, J. G. S. Duque, R. R. Urbano, C. Rettori, J. D. Thompson, M. F. Hundley, and J. L. Sarrao, J. Appl. Phys. **99**, 08P703 (2006).
[14] P. G. Pagliuso, J. D. Thompson, M. F. Hundley, J. L. Sarrao, and Z. Fisk, Phys. Rev. B **63**, 054426 (2001).
[15] Z. Fisk and J. P. Remeika, *Handbook on the Physics and Chemistry of Rare Earths* (Elsevier, North-Holland, 1989), Vol. 12, p. 53.
[16] T. C. Kobayashi, H. Hidaka, H. Kotegawa, K. Fujiwara, and M. I. Eremets, Rev. Sci. Instrum. **78**, 023909 (2007).
[17] C. Adriano, Ph.D. thesis, Instituto de Física "Gleb Wataghin," UNICAMP, 2009.
[18] J. Rusz, P. M. Oppeneer, N. J. Curro, R. R. Urbano, B.-L. Young, S. Lebegue, P. G. Pagliuso, L. D. Pham, E. D. Bauer, J. L. Sarrao, and Z. Fisk, Phys. Rev. B **77**, 245124 (2008).
[19] H. Hegger, C. Petrovic, E. G. Moshopoulou, M. F. Hundley, J. L. Sarrao, Z. Fisk, and J. D. Thompson, Phys. Rev. Lett **84**, 4986 (2000).
[20] M. Nicklas, V. A. Sidorov, H. A. Borges, P. G. Pagliuso, C. Petrovic, Z. Fisk, J. L. Sarrao, and J. D. Thompson, Phys. Rev. B **67**, 020506(R) (2003).
[21] W. Bao, P. G. Pagliuso, J. L. Sarrao, J. D. Thompson, Z. Fisk, and J. W. Lynn, Phys. Rev. B **64**, 020401(R) (2001).
[22] G. L. Squires, *Introduction to the Theory of Thermal Neutron Scattering* (Dover, Mineola, NY, 1996).
[23] G. Shirane, S. M. Shapiro, and J. M. Tranquada, *Neutron Scattering with a Triple-Axis Spectrometer, Basic Techniques* (Cambrige University Press, Cambridge, 2002).
[24] M. Blume, A. J. Freeman, and R. E. Watson, J. Chem. Phys. **37**, 1245 (1962).
[25] C. Adriano, P. F. S. Rosa, C. B. R. Jesus, J. R. L. Mardegan, T. M. Garitezi, T. Grant, Z. Fisk, D. J. Garcia, A. P. Reyes, P. L. Kuhns, R. R. Urbano, C. Giles, and P. G. Pagliuso, Phys. Rev. B **90**, 235120 (2014).
[26] C. Adriano, P. F. S. Rosa, C. B. R. Jesus, T. Grant, Z. Fisk, D. J. Garcia, and P. G. Pagliuso, J. Appl. Phys. **117**, 17C103 (2015).
[27] P. F. S. Rosa, R. J. Bourg, C. B. R. Jesus, P. G. Pagliuso, and Z. Fisk, Phys. Rev. B **92**, 134421 (2015).
[28] R. Lora-Serrano, C. Giles, E. Granado, D. J. Garcia, E. Miranda, O. Aguero, L. Mendonça Ferreira, J. G. S. Duque, and P. G. Pagliuso, Phys. Rev. B **74**, 214404 (2006).
[29] A. Malinowski, M. F. Hundley, N. O. Moreno, P. G. Pagliuso, J. L. Sarrao, and J. D. Thompson, Phys. Rev. B **68**, 184419 (2003).